2014

Dynamic Performance Of A Compression Thermoelastic Cooling Air-Conditioner Under Cyclic Operation Mode

Suxin Qian
University of Maryland, College Park, United States of America, sqian@umd.edu

Jiazhen Ling
University of Maryland, College Park, United States of America, jiazhen@umd.edu

Yunho Hwang
University of Maryland, College Park, United States of America, yhhwang@umd.edu

Reinhard Radermacher
University of Maryland, College Park, United States of America, raderm@umd.edu

Dynamic Performance of a Compression Thermoelastic Cooling Air-Conditioner under Cyclic Operation Mode

Suxin QIAN[1], Jiazhen LING[1], Yunho HWANG*, Reinhard RADERMACHER[1]

[1]Center for Environmental Energy Engineering, Department of Mechanical Engineering, University of Maryland, 4164 Glenn L. Martin Hall Bldg., College Park, MD 20742, USA

Tel: (+1) 301-405-5247, Fax: (+1) 301-405-2025, Email: yhhwang@umd.edu

* Corresponding Author

ABSTRACT

Traditional vapor compression cooling refrigerants are considered to have high global-warming-potential (GWP), which face more and more legislation pressure nowadays. As an alternative option other than using low GWP refrigerants and natural refrigerants, solid-state cooling technologies show their advantages of zero GWP, and therefore recently attract more attentions. Apart from those well-studied solid-state cooling technologies, such as thermoelectric cooling, thermoacoustic cooling and magnetic cooling, thermoelastic cooling, a.k.a. elastocaloric cooling, is still under development and shows potential of better thermal performance compared with its competitors. In fact, from material perspective, it was estimated by literatures that the COPs for elastocaloric materials are 20% - 120% higher than other solid-state cooling materials under the same operating conditions. This study introduces the thermoelastic cooling concept at the beginning, and then demonstrates one method to operate the compression thermoelastic cooling cycle for air-conditioning application based on the reverse Martensitic phase transition principle. A dynamic model is developed to measure the temperature within the cycle under cyclic operation mode. The cyclic operation is a reversed Brayton cycle consisting of an adiabatic Martensite-Austenite phase transition process, a constant strain heat transfer process between the solid-state refrigerant and the heat sink/source, and a heat recovery process aiming to improve the overall performance. The model uses experimental curve-fitted data to predict the work required to drive the cycle. Based on the model, cooling COP of 4 is achievable under a 10K temperature lift case.

1. INTRODUCTION

Traditional refrigerants used for vapor compression cooling systems with large global warming potential are facing more and more legislation pressures nowadays. Solid-state cooling technologies, including magnetic cooling, thermoacoustic cooling, and thermoelectric cooling are considered as possible alternatives for vapor compression cooling systems. Recently, thermoelastic cooling (a.k.a. elastocaloric cooling) have been proposed as a new solid-state cooling technology (Cui et al., 2012) with potential performance improvements to state-of-the-art vapor compression cooling systems. In fact, from a material perspective, thermoelastic cooling is even much better than magnetic cooling since the temperature span is large enough so that a single stage heat pump cycle is enough, rather than complicated cascade cycle widely used in magnetic cooling field.

The thermoelastic effect is associated with the Martensitic phase change process for the so-called shape memory alloys (SMAs). Figure 1 is an illustration of the stress induced Martensitic phase change process and how it is compared to the liquid-vapor phase change process. Figure 1 (c) shows a condensation process (below critical point) induced by pressure difference, during which vapor becomes liquid if the applied system pressure (vapor pressure) is higher than the saturated pressure at the system temperature. During the adiabatic condensation process, the liquid temperature increases due to the released latent heat. Similarly in Figure (a), there are two solid phases corresponding to two different crystals. Austenite becomes Martensite when subjected to a system stress higher than the "saturation stress" corresponding to the current system temperature. The released latent heat heats up the solid itself during the adiabatic phase change process. The reversed process is shown in Figure 1 (b), when the applied system stress is less than the "saturation stress". For example, when the force is released, the Martensite transforms to Austenite and absorbs latent heat from itself by reducing the temperature. This stress induced temperature drop is the thermoelastic cooling effect. The most widely used SMAs with significant thermoelastic cooling effect are NiTi alloy, CuZnAl alloy (Bonnot et al., 2008), and CuAlNi alloy (Picornell et al., 2004).

This paper introduces how to achieve continuous cooling from this thermoelastic cooling effect by demonstration of a reversed Brayton cycle design first. The performance of the studied thermoelastic cooling system is investigated by a dynamic model developed in this study.

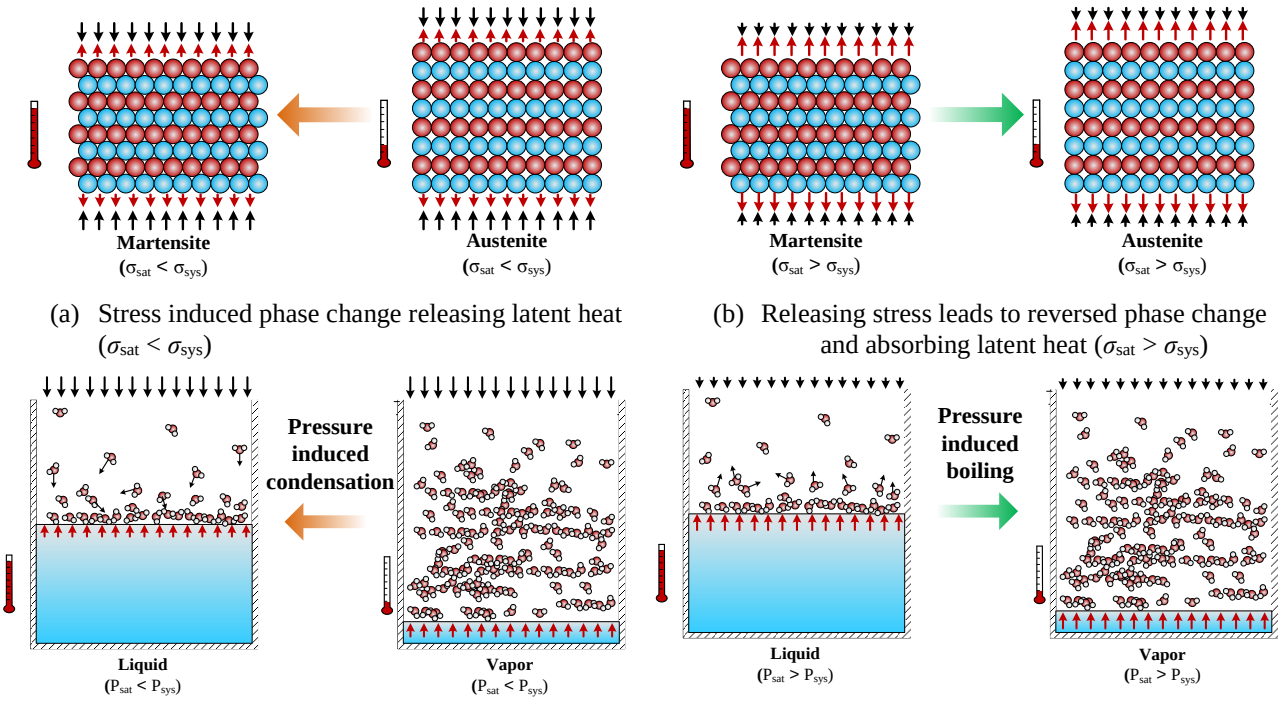

(a) Stress induced phase change releasing latent heat ($\sigma_{sat} < \sigma_{sys}$)

(b) Releasing stress leads to reversed phase change and absorbing latent heat ($\sigma_{sat} > \sigma_{sys}$)

(c) Pressure induced condensation releasing latent heat ($P_{sat} < P_{sys}$)

(d) Pressure induced boiling absorbing latent heat ($P_{sat} > P_{sys}$)

Figure 1: Illustration of stress induced Martensitic phase transformation process, a.k.a. elastocaloric or thermoelastic effect in a SMA material and comparison to adiabatic liquid/vapor phase change.

2. THERMOELASTIC COOLING CYCLE DESCRIPTION

Following the tradition of thermodynamic analysis, a reversible thermoelastic cooling cycle is plotted on a T-S diagram and a stress-strain (σ-ε) diagram to demonstrate its working principle, as shown in Figure 2. Given the context of vapor compression cycle, a σ-ε is similar to the pressure-specific volume diagram, since stress has the

same unit with pressure and both diagrams are used to analyze works associated with the specific thermodynamic cycle. The ideal reversible cycle plotted in Figure 2 is a reversed Brayton cycle, which consists of two isentropic processes and two iso-stress (isobaric) processes. It starts from state at unstressed state 1. The loading process (1→1'→2) is isentropic from Austenite to Martensite phase, since applied system stress is greater than the "saturation stress" ($\sigma_{sat} < \sigma_{sys}$). Process 1→1' is a single phase loading while the stress inside crystal is still less than the "saturation stress" at that temperature T_1. Phase change is undergoing from 1'→2, and the stress increasing is due to "saturation stress" increasing caused by temperature rising from 1→2 on the T-S diagram. The SMA is then cooled down (2→3) approaching the heat sink's temperature at T_h (ambient for a cooling cycle) while still loaded. Before fully unstressed, the SMA is further cooled down to state 4 via the heat recovery process, by changing the sensible heat from the current SMA to another set of SMA at state 6. Process 4→4'→5 is the reversed isentropic phase change process when the stress is released, since the "saturation stress" is now greater than system stress ($\sigma_{sat} > \sigma_{sys}$). Again 4→4' is the single phase unloading process, and 4'→5 is corresponding to the reversed phase change process. The SMA's cooling power is then taken away from 5→6 approaching the heat source's temperature T_c (conditioned space temperature for a cooling cycle). While unstressed, the heat recovery process 6→1 finishes the whole cycle.

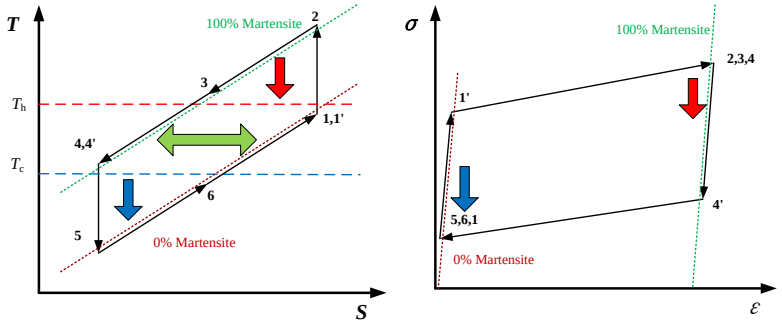

Figure 2: Illustration of reversed Brayton cycle and its variation as a thermoelastic cooling cycle.

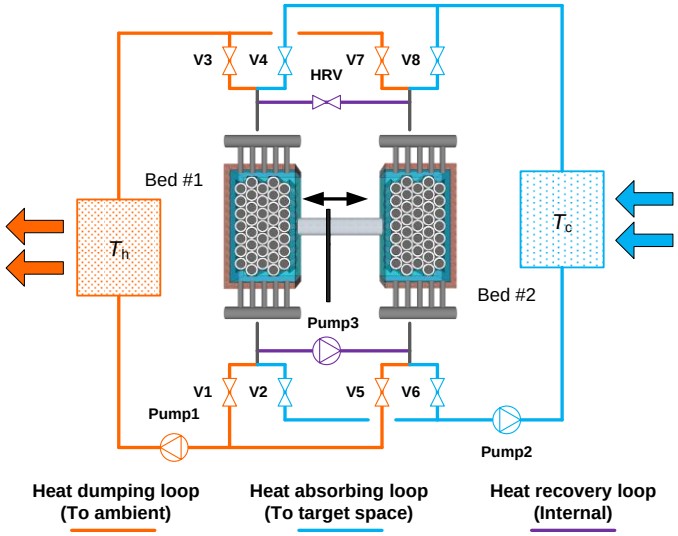

Figure 3: Schematic of the specific thermoelastic cooling system heat transfer fluid loop used for the numerical model.

The above Brayton cycle design could be achieved by the schematic in Figure 3. Here, water is used as the heat transfer fluid to achieve cooling SMA (2→3 in Figure 2), heating SMA (5→6) and internal heat recovery (3→4 and 6→1), as indicated by different colors in the schematic. There are two SMA beds, a heat sink T_h to reject heat, and a

heat source T_c to absorb heat from conditioned space. The corresponding loops are only active when they are needed. For example, the left side heat dumping loop (orange loop) consists of V1, V3 and Pump1, and they are turned on when Bed 1 needs to be cooled to T_h (process 2→3 in Figure 2), and is not active during the rest of the cycle. A detailed valves and pumps sequence is specified in Table 1. Since the valves and pumps are switched periodically between cycles, we call the designed thermoelastic cooling system operating under cyclic operation mode.

Table 1: Valves and pumps sequence of the specific thermoelastic cooling system model.

Process in Figure 2	1→2	2→3	3→4	4→5	5→6	6→1
V1	X	O	X	X	X	X
V2	X	X	X	X	O	X
V3	X	O	X	X	X	X
V4	X	X	X	X	O	X
V5	X	X	X	X	O	X
V6	X	O	X	X	X	X
V7	X	X	X	X	O	X
V8	X	O	X	X	X	X
HRV	X	X	O	X	X	O
Pump1	X	O	X	X	O	X
Pump2	X	O	X	X	O	X
Pump3	X	X	O	X	X	O

Note: "X" is close/off, "O" is open/on.

3. MODEL DEVELOPMENT

A dynamic model is developed to evaluate the specified thermoelastic cooling system performance according to schematic in Figure 3. We use a specific NiTi alloy tube (nitinol tube) as the material for SMA beds, and the basic properties needed for the model are listed in Table 2.

Table 2: Physical properties and loading/unloading parameters of NiTi alloy nitinol. (*)

Refrigerant alloy	NiTi
Density (kg/m^3)	6400-6500 (6500)
Specific heat (J/kg·K)	470-620 (550)
Conductivity (W/m·K)	8.6-18 (18)
Entropy change Δs (J/kg·K)	42
ΔT_{ad} (K)	22.9 (measured at 300 K)
Transformation temperature (°C)	-200 –200
Uniaxial loading work w_+ (J/g)	3.94 (Compressive)
Uniaxial unloading work w_- (J/g)	2.92 (Compressive)
Net work with recovery (J/g)	1.02 (Compressive)
Data source	Cui et al., 2012, Smith et al., 1993, Otsuka and Wayman 1998

* The numbers in bracket are specific numbers used for all calculation in this study.

Here are several assumptions of the model:

- Martensitic phase transformation time scale and loading time scale is negligible compared with heat transfer time scale.
- Radial heat transfer time scale is negligible compared with axial direction, $Bi_\delta < 0.01$
- Uniaxial loading and uniform phase transformation
- Constant thermophysical properties within the small temperature range of interest
- Incompressible flow and uniform velocity profile at any cross section inside the nitinol tube
- Uniform fluid temperature profile at any cross section inside the nitinol tube
- No heat transfer from nitinol tubes to surrounding

The core part of this model is the SMA bed, or the nitinol tube. The temperature at any time of the solid nitinol tube, and the water inside it are predicted by the energy equation in Eq. (1) and (2). Eq. (1) shows the energy equation for solid, which consists of conduction term, convection interaction with water term, and generation term. The third term, i.e. generation term becomes zero if there is no phase change, is positive if we have Austenite to Martensite phase change, and is negative if we have Martensite to Austenite phase change, as described in Eq. (3).

$$\frac{\partial T_m}{\partial t} = \alpha_m \frac{\partial^2 T_m}{\partial x^2} - \frac{h}{\delta \cdot \left(\rho c_p\right)_m}\left(T_m - T_f\right) + \frac{g'''}{\left(\rho c_p\right)_m} \tag{1}$$

$$\frac{\partial T_f}{\partial t} = \alpha_f \frac{\partial^2 T_f}{\partial x^2} - \frac{4h}{ID \cdot \left(\rho c_p\right)_f}\left(T_f - T_m\right) - u_f \frac{\partial T_f}{\partial x} \tag{2}$$

$$g''' = \begin{cases} \rho\left(\Delta H + w_+\right)\dot{\xi} & \dot{\xi} \geq 0 \\ \rho\left(\Delta H + w_-\right)\dot{\xi} & \dot{\xi} < 0 \end{cases} \tag{3}$$

Note that since we assume that the phase transition time scale is small enough to be ignored, a quasi-steady state phase change approximation to be reasonable. In other words, the phase fraction change rate is simplified to a constant during the loading/unloading process.

The heat source and sink are modeled as lump systems according to Eq. (4), similar to a water tank without considering stratification. Since we assume incompressible water, there is no mass accumulation/reduction inside heat source or sink. The second term on the right hand side indicates the heater's capacity for heat source, or cooler's capacity for heat sink. In reality, it should be the heat exchanger capacity between the water to the air (ambient/conditioned space).

$$m_c c_{p,f} \frac{dT_c}{dt} = \dot{m}_c c_{p,f}\left(T_{in} - T_c\right) + \dot{Q}_c \tag{4}$$

The rest of the system are pipes. Multi-nodes model is used rather than single node to capture the transient temperature change more precisely, especially when the time scale becomes smaller under some operating conditions, as shown in Eq. (5-6). The thermal mass factor κ in Eq. (6) is to take account of pipe wall dead thermal mass, which is a "resistance" or a loss to the cooling power delivery.

$$\frac{\partial T_f}{\partial t} = \frac{k_f}{\kappa\left(\rho c_p\right)_f}\frac{\partial^2 T_f}{\partial x^2} - \frac{4h_{air}}{\kappa\left(\rho c_p\right)_f OD}\left(T_f - T_{amb}\right) - \frac{u_f}{\kappa}\frac{\partial T_f}{\partial x} \tag{5}$$

$$\kappa = \frac{\left(mc_p\right)_f + \left(mc_p\right)_s}{\left(mc_p\right)_f} = \frac{\left(\rho c_p\right)_f ID^2 + \left(\rho c_p\right)_s\left(OD^2 - ID^2\right)}{\left(\rho c_p\right)_f ID^2} \tag{6}$$

$$\bar{\dot{Q}}_c = \frac{\int_0^{t_{cyc}} \dot{Q}_c \mathrm{d}t}{t_{cyc}} \tag{7}$$

$$COP = \frac{\bar{\dot{Q}}_c t_{cyc}}{W_+ - W_-}\eta_{mech} \tag{8}$$

The system cooling capacity is evaluated based on the heat source's time averaged capacity during the cycle. COP is then evaluated based on capacity and work required to finish a cycle. 85% mechanical efficiency is assumed here in Eq. (8).

4. RESULTS AND DISCUSSION

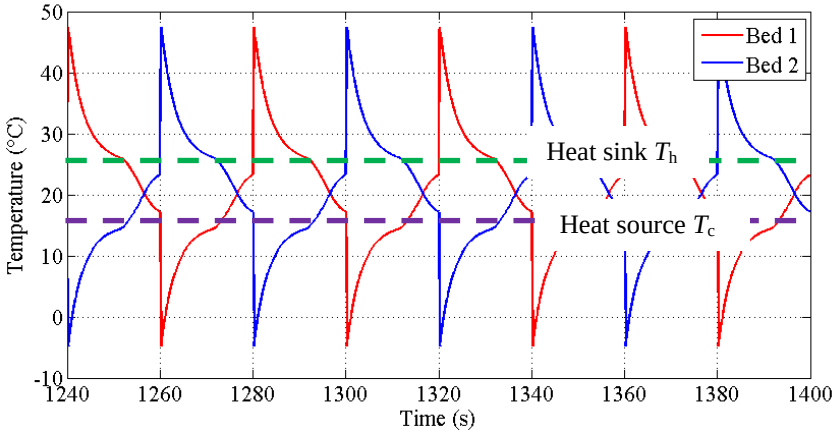

Figure 4: Temperature profiles of two SMA beds during the cyclic steady state data sampling period.

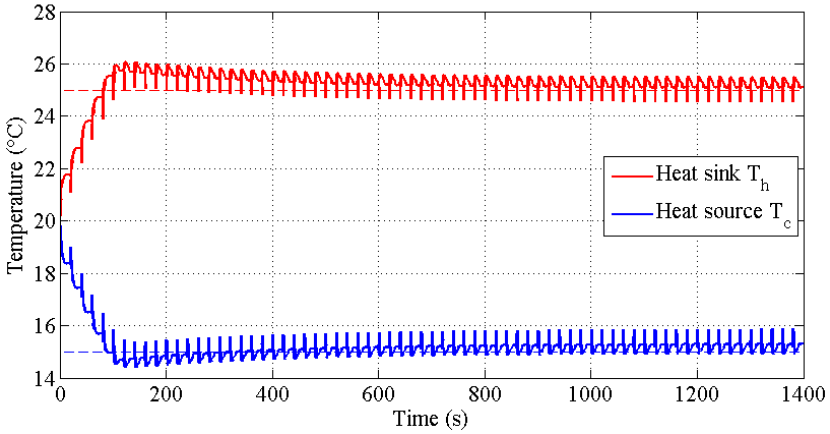

Figure 5: Demonstration of temperature profiles of heat source and heat sink (dashed lines are set points).

Figure 4 demonstrates the temperature profiles of two NiTi tube beds over four cooling cycles during the "cyclic steady state" period. The "cyclci steady state" refers to the period during which the two beds' temperature curves shape do not change between cycles. The temperature curves follow exactly the same cycle plotted on the T-S diagram in Figure 2. The almost vertical temperature jump/drop is due to the Martensitic phase change process (process 1→2 or 4→5 in Figure 2). The exponential alike curve afterwards is the heat absorbing/rejection process (2→3 or 5→6). The second exponential alike curve after the NiTi bed approaches temperatures of heat source/sink is the heat recovery process (3→4 or 6→1). Figure 5 shows the temperature profiles of heat sink T_h and heat source T_c, respectively. The two dashed lines are setpoints for these two heat exchangers, controlled by two imaginary PID controllers. The corresponding temperature lift is 10K in this case. One important finding here is that the warming

up process is fast, which is less than 3 minutes. It takes around 1000 seconds to reach "cyclic steady state" in this specific case.

Figure 6 shows the capacity profile of heat sink and heat source. Here, the two dashed lines are the time averaged capacities sampled during the "cyclic steady state" period. In this scenario, the cooling capacity is 65 W.

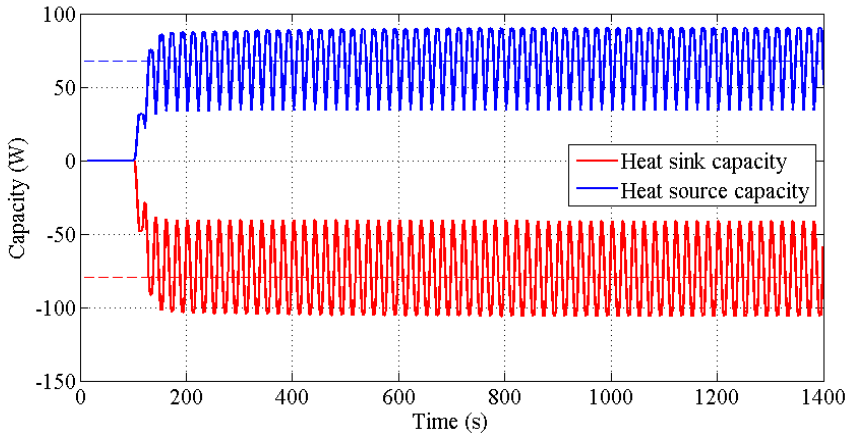

Figure 6: Heat source and heat sink capacity variation with time (dashed lines are time averaged capacity sampled during the cyclic steady state period).

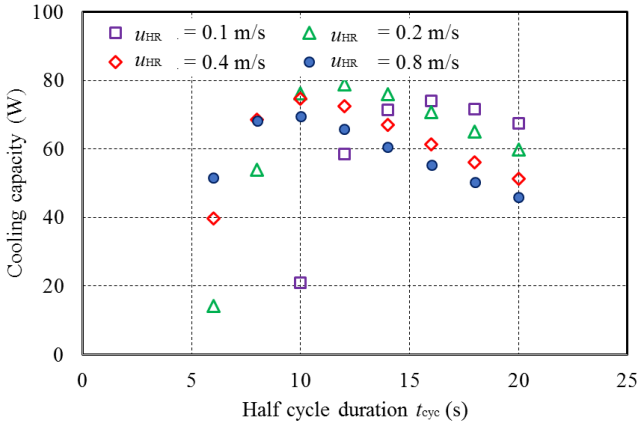

Figure 7: Cooling capacity as a function of half cycle duration.

To understand how the system performance varies, we plot the cooling capacity and COP as a function of cycle duration, as shown in Figure 7 and 8 respectively. Figure 7 indicates that an optimum cycle duration exists for cooling capacity, but is not a constant when the heat recovery flow velocity changes. This trade off is easy to understand, since a longer cycle duration generates more cooling capacity per cycle due to a more effective heat trasnfer, but loses capacity when cycling slower. The second message is not that clear. By comparing four different curves with different heat recovery heat transfer fluid velocity over NiTi bed, the maximum capacity is higher than other three cases when the heat recovery flow velocity is 0.2 m/s. This flow rate wise optimum is due to the fact that the cooling capacity is also strongly dependent on the heat recovery efficiency Previous study indicated that heat recovery efficiency favors slower heat recovery flow velocity u_{HR} since it's more reversible. However, a slower u_{HR} requires more time for heat recovery, and limits the available time for heat transfer and heat transfer effectiveness. As a result, heat transfer is the limiting factor for short cycle duration cases, where a higher heat recovery flow rate leads to better performance. On the other hand, heat recovery is the limiting factor for longer cycle duration cases,

where a slower heat recovery flow rate results in better performance. From COP point of view, a more effective heat transfer and a more reversible heat recovery always help to increase COP. That's the interpretation of Figure 8, that COP favors longer cycle duration.

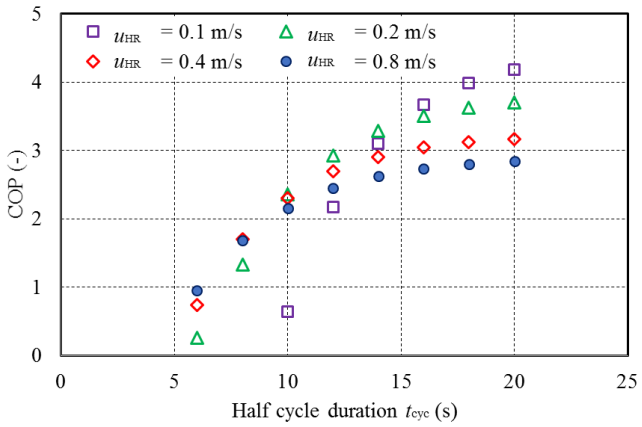

Figure 8: COP as a function of half cycle duration.

5. CONCLUSIONS

This paper introduces the new cooling concept – thermoelastic cooling, by demonstrating one way to take advantage of the thermoelastic effect and how to design a thermoelastic cooling system based on Brayton cycle operating principle. A dynamic model is developed to quantitatively understand the performance of the designed system and make predictions for future studies. The predicted temperature profiles and capacities curves from the dynamic model look physically reasonable. A simple parametric study is conducted to study the role of cycle frequency on the COP and cooling capacity. It is found that an optimum cycle duration and heat recovery flow rate exist for cooling capacity, while COP favors longer cycle duration and smaller heat recovery flow rate when the cycle duration is appropriate. Based on the model, COP of 4 could be achieved at a 10 K water-water system temperature lift.

NOMENCLATURE

Symbols

Bi	Biot number	(-)
COP	Coefficient of performance	(-)
c_p	Specific heat	($J \cdot kg^{-1} \cdot K^{-1}$)
D	Diameter	(m)
ε	Strain	(-)
GWP	Global warming potential	
g'''	Generation term	(W/m^3)
HR	Heat recovery (regeneration)	
ΔH	Latent heat	($J \cdot kg^{-1}$)
h	Heat transfer coefficient	($W \cdot m^{-2} \cdot K^{-1}$)
k	Thermal conductivity	($W \cdot m^{-1} \cdot K^{-1}$)
L	Length	(m)

m	Mass	(kg)
$\dot{m}$	Mass flow rate	($kg \cdot s^{-1}$)
$\dot{Q}$	Capacity	(W)
S	Entropy	($J \cdot kg^{-1} \cdot K^{-1}$)
SMA	Shape memory alloy	
T	Temperature	(°C)
t	Time	(sec)
u	Fluid velocity	($m \cdot s^{-1}$)
w	Specific work	($J \cdot g^{-1}$)
$\dot{W}$	Work rate	(W)
α	Thermal diffusivity	($m^2 \cdot s^{-1}$)
σ	Stress	(MPa)
κ	Thermal mass factor	(-)
ρ	Density	($kg \cdot m^{-3}$)
ξ	Martensite phase fraction	(-)
Subscript		
ad	adiabatic	
cyc	cycle	
f	fluid	
HT	heat transfer	
mech	mechanical	
mot	motor	
rec	recovery	
S	solid	
+	loading	
-	unloading	

REFERENCES

Bonnot, E., Romero, R., Manosa, L., Vives, E., Planes, A., 2008, Elastocaloric Effect Associated with the Martensitic Transition in Shape-Memory Alloys, Phys. Rev. Lett., doi: 10.1103/PhysRevLett.100.125901.

Cui, J., Wu, Y., Muehlbauer, J., Hwang, Y., Radermacher, R., Fackler, S., et al., 2012, Demonstration of High Efficiency Elastocaloric Cooling with Large Delta-T Using NiTi Wires, *Appl. Phys. Lett.*, doi: 10.1063/1.4746257.

Otsuka, K., and Wayman, C.M., 1998, *Shape Memory Materials*, Cambridge University Press, Cambridge, p. 174-177.

Picornell, C., Jaime, P., Cesari, E., 2004, Stress-Temperature Relationship in Compression Mode in Cu-Al-Ni Shape Memory Alloys, Mater. Trans., vol.45:p.1679-83.

Smith, J.F., Luck, R., Jiang, Q., Predel, B., 1993, The Heat Capacity of Solid Ni-Ti Alloys in the Temperature Range 120 to 800 K. *J. Ph. Equailib*., vol.14:p.494-500.

ACKNOWLEDGEMENT

The authors gratefully acknowledge the support of this effort from the U.S. DOE and the Center for Environmental Energy Engineering (CEEE) at the University of Maryland. This work was supported by DOE ARPA-E DEAR0000131.